

**Isobaric yield ratios and the symmetry energy in heavy-ion reactions near the Fermi energy**M. Huang,<sup>1,2,3</sup> Z. Chen,<sup>1,2</sup> S. Kowalski,<sup>4</sup> Y. G. Ma,<sup>5</sup> R. Wada,<sup>1,\*</sup> T. Keutgen,<sup>6</sup> K. Hagel,<sup>1</sup> M. Barbui,<sup>1</sup> A. Bonasera,<sup>1,7</sup> C. Bottosso,<sup>1</sup> T. Materna,<sup>1</sup> J. B. Natowitz,<sup>1</sup> L. Qin,<sup>1</sup> M. R. D. Rodrigues,<sup>1</sup> P. K. Sahu,<sup>1</sup> and J. Wang<sup>2</sup><sup>1</sup>*Cyclotron Institute, Texas A&M University, College Station, Texas 77843, USA*<sup>2</sup>*Institute of Modern Physics, Chinese Academy of Sciences, Lanzhou, 730000, People's Republic of China*<sup>3</sup>*Graduate University of Chinese Academy of Sciences, Beijing 100049, People's Republic of China*<sup>4</sup>*Institute of Physics, Silesia University, Katowice, Poland*<sup>5</sup>*Shanghai Institute of Applied Physics, Chinese Academy of Sciences, Shanghai 201800, People's Republic of China*<sup>6</sup>*FNRS and IPN, Université Catholique de Louvain, B-1348 Louvain-Neuve, Belgium*<sup>7</sup>*Laboratori Nazionali del Sud, INFN, via Santa Sofia, 62, 95123 Catania, Italy*

(Received 25 January 2010; revised manuscript received 3 April 2010; published 30 April 2010)

The relative isobaric yields of fragments produced in a series of heavy-ion-induced multifragmentation reactions have been analyzed in the framework of a modified Fisher model, primarily to determine the ratio of the symmetry energy coefficient to the temperature,  $a_{\text{sym}}/T$ , as a function of fragment mass  $A$ . The extracted values increase from 5 to  $\sim 16$  as  $A$  increases from 9 to 37. These values have been compared to the results of calculations using the antisymmetrized molecular dynamics (AMD) model together with the statistical decay code GEMINI. The calculated ratios are in good agreement with those extracted from the experiment. In contrast, the values extracted from the ratios of the primary isobars from the AMD model calculation are  $\sim 4$  to 5 and show little variation with  $A$ . This observation indicates that the value of the symmetry energy coefficient derived from final fragment observables may be significantly different than the actual value at the time of fragment formation. The experimentally observed pairing effect is also studied within the same simulations. The Coulomb coefficient is also discussed.

DOI: [10.1103/PhysRevC.81.044620](https://doi.org/10.1103/PhysRevC.81.044620)

PACS number(s): 25.70.Pq

**I. INTRODUCTION**

In the early 1980s, a study of the isotopic-yield distributions of intermediate mass fragments produced in high-energy proton-induced multifragmentation reactions at Fermi Lab showed that the distributions can be well described by a modified Fisher model (MFM) [1,2] in which the isotope production is governed by the available free energy. Therefore, isotopic yields provide a good probe for studying the nature of the disassembling nuclear system. Multifragmentation of the system is also generally observed in violent collisions in heavy-ion reactions in the Fermi-energy domain and there is evidence that both subnormal and supernormal densities may be explored in such collisions [3,4]. Works in this area have concentrated on exploring the nuclear equation of state and the liquid-gas phase transition in nuclear matter. In a previous article we addressed the possibility of probing the quantum nature of the liquid-gas phase transition using isotopic yield distributions [5].

Over the past several years, many fragment emission studies have been motivated by efforts to use fragment yield distributions, either singly or by comparison to those of similar reactions, to explore the symmetry energy in the emitting source at different densities and temperatures [3,6–9]. In each of these cases, measuring the isotopic yield distributions over a wide range of mass number  $A$  and atomic number  $Z$  should provide a more reliable basis for extraction of the desired information. Even then there are important issues that must be resolved to establish the relation between the

experimental isotopic yield distributions and the symmetry energy of the emitting system. One is the source temperature  $T$ . In the MFM, as well as other approaches based upon the free energy, all terms that can be determined from experiments appear in the form of  $a_i/T$  times some function of  $A$ ,  $Z$ , or the neutron number  $N$ , where  $i$  indicates the coefficient of the different terms contributing to the free energy. Since the beginning of the experimental study of heavy-ion collisions in the multifragmentation regime, significant efforts have been made to evaluate the source temperature, but no absolute consensus among different methods has yet been achieved [10]. A second issue is the role and effect of secondary decay processes. In experiments the majority of the detected fragments are in their ground states. Most of the primary fragments produced in Fermi-energy heavy-ion reactions are expected to be in an excited state when they are formed. Indeed, in previous works, excitation energies of the primary fragments have been evaluated by studying the associated light charged-particle multiplicities [11,12]. Such data demonstrate that secondary decay is important and raise the question of the degree of confidence that can be accorded to experimental derivations of the symmetry energy coefficient that do not properly correct for this important effect. A clear goal for experimentalists would be the reconstruction of the primary isotopic yield distributions from the experimental distributions. This might be approached by a reconstruction of the primary isotope distributions employing the associated neutron and charged-particle multiplicities. However, because multiple fragments are produced in a reaction and light particles can be produced even before the formation of the fragments, the identification of the parent for a detected light

\*wada@comp.tamu.edu

particle observed in coincidence with detected fragments is not straightforward. A reconstruction of the primary isotope distribution was part of goal of the experiment described here, but that analysis is still under way [13]. A third issue, not addressed in this article but of critical importance in this field, is the problem of obtaining reliable estimates of the density at the time of fragment formation. In the absence of such information most density estimates should be viewed as unconfirmed. While this may be somewhat mitigated by comparing experimental observables with results of dynamic models employing particular assumed forms for the density dependence of the symmetry energy, such approaches are integral and may be influenced by other assumptions and parameter choices inherent in the model applied [14].

In the works of the Purdue Group [1,2], the experimental isotopic yield distributions have been well reproduced by MFM. In these, nine parameters are involved, and one of them (the volume coefficient, typically) is arbitrarily fixed to the nominal ground-state value. However, there is no reason for any parameters to be same as the nominal ground-state values. Each parameter depends not only on the temperature, but also on the density of the emitting source, and furthermore the secondary sequential decay effects may significantly modify the values. These issues make it very difficult to pursue the physical meaning of the extracted parameters, even though the isotopic yield distributions are well reproduced by a single set of parameters. Instead of attempting to determine a unique set of the parameters globally, parameters are related to the isobaric yields in the framework of MFM. In the ratios between the same mass of fragments many terms cancel out and one can study the specific terms individually and discuss the meaning of the extracted parameters more clearly. We used MFM to relate the experimental isobaric yield ratios to the parameters. One can also perform a similar analysis, using a ground canonical approach [8,15], where one needs to calculate the statistical weight factors for the excited fragments. This calculation is not straightforward, because the fragments are formed in the emitting source of temperature  $T$  and the experimentally available level scheme is not well established for the fragments away from the  $\beta$ -stability line. This is one reason we chose MFM. Another reason for choosing MFM is that, as discussed in Ref. [5], the isotopic yields show a power law distribution for a given  $I = N - Z$  value and MFM is a natural choice for reproducing such distributions. To pursue the physical meanings of the extracted values, they are compared with those that are extracted in the same way from simulations, for both the primary excited fragments and the final ground-state ones. The antisymmetrized molecular dynamics (AMD) model of Ono *et al.* is used with a statistical decay code GEMINI as an afterburner [9,16–18]. In this article we explore the extent to which information on the symmetry energy, in the form of  $a_{\text{sym}}/T$ , can be extracted from high-quality data for isotopically resolved fragment-yield distributions and compared to the model predictions [9,19]. The role of the secondary decay is explored by comparisons with results of theoretical calculations. In a separate article we discuss the extraction of such information using isoscaling techniques [20].

## II. EXPERIMENT

The experiment was performed at the K-500 superconducting cyclotron facility at Texas A&M University.  $^{64,70}\text{Zn}$  and  $^{64}\text{Ni}$  beams were used to irradiate  $^{58,64}\text{Ni}$ ,  $^{112,124}\text{Sn}$ ,  $^{197}\text{Au}$ , and  $^{232}\text{Th}$  targets at 40 A MeV. Intermediate mass fragments (IMFs) were detected by a detector telescope placed at  $20^\circ$ . The telescope consisted of four Si detectors. Each Si detector was  $5 \times 5$  cm. The nominal thicknesses were 129, 300, 1000, and 1000  $\mu\text{m}$ . All Si detectors were segmented into four sections and each quadrant had a  $5^\circ$  opening angle in polar and azimuthal angles. Therefore, the energies of the fragments were measured at two polar angles of the quadrant detector, namely,  $\theta = 17.5^\circ \pm 2.5^\circ$  and  $\theta = 22.5^\circ \pm 2.5^\circ$ . Typically, six to eight isotopes for atomic numbers  $Z$  to  $Z = 18$  were clearly identified with the energy threshold of 4–10 A MeV, using the  $\Delta E - E$  technique for any two consecutive detectors. The  $\Delta E - E$  spectrum was linearized empirically. Mass identification of the isotopes were made using a range-energy table [21]. In the analysis code, isotopes are identified by a parameter  $Z_{\text{real}}$ . For the isotope with  $A = 2Z$ ,  $Z_{\text{real}} = Z$  is assigned and other isotopes are identified by interpolation between them. Typical  $Z_{\text{real}}$  spectra are shown in Fig. 1. The energy spectrum of each isotope was extracted by gating the isotope in a two-dimensional (2D) plot of  $Z_{\text{real}}$  vs energy. The yields of light charged particles (LCPs) in coincidence with IMFs were also measured using 16 single-crystal CsI(Tl) detectors of 3 cm thickness set around the target. The light output from each detector was read by a photomultiplier tube. The pulse shape discrimination method was used to identify  $p$ ,  $d$ ,  $t$ ,  $h$ , and  $\alpha$  particles. The energy calibrations for these particles were performed using Si detectors (50–300  $\mu\text{m}$ ) in front of the CsI detectors in separate runs.

The yield of each isotope was evaluated, using a moving source fit. For LCPs, three sources [projectilelike fragments (PLFs), nucleon-nucleon ( $NN$ )-like, and targetlike fragments

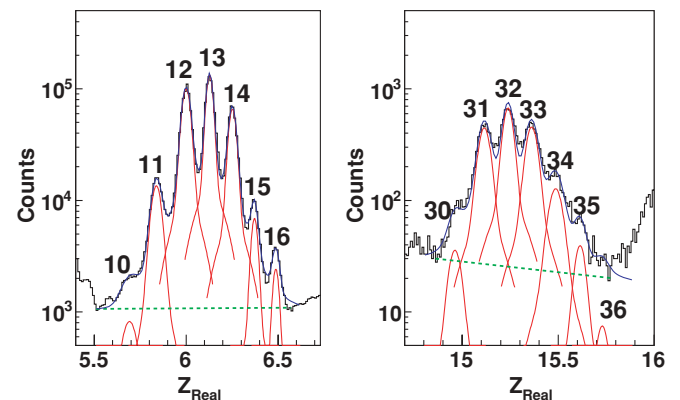


FIG. 1. (Color online) Typical linearized isotope spectra for  $Z = 6$  and 15 are shown for  $^{64}\text{Ni} + ^{124}\text{Sn}$ . The number at the top of each peak is the assigned mass number. The histograms depict experimental data. A linear background is assumed from valley to valley for a given  $Z$ . Each isotope is fit with two Gaussians. The individual fit indicates the yield of the isotope above the background. The sum of Gaussians and the background are also shown in each spectrum.

(TLFs)] were used. The  $NN$ -like sources have source velocities of about a half of the beam velocity. The parameters are searched globally for all 16 angles. For IMFs, because the energy spectra were measured only at the two angles of the quadrant detector, the spectra were parametrized using a single  $NN$  source. Using a source with a smeared source velocity around half the beam velocity, the fitting parameters were first determined from the spectrum summed over all isotopes for a given  $Z$ , assuming  $A = 2Z$ . Then all extracted parameters except for the normalizing yield parameter were used for the individual isotopes. This procedure was based on the assumption that, when the spectrum is plotted in energy per nucleon, the shape of the energy spectrum is same for all isotopes for a given  $Z$ . Because the yield of the energy spectra are dominated in the lower-energy side, slightly different temperatures from some of the isotopes with high statistics results in the yield within the error bars given in what follows. For the IMFs, a further correction was made for the background. As seen in Fig. 1, the isotopes away from the stability line, such as  $^{10}\text{C}$  and  $^{36}\text{P}$ , have a very small yields and the background contribution is significant. To evaluate the background contribution to the extracted yield from the source fit, a two-Gaussian fit to each isotope combined with a linear background was used. The fits are shown in Fig. 1. Each peak consists of two Gaussians. The second Gaussian (about 10% of the height of the first one) is added to reproduce the shape of the valley between two isotopes. This component is attributed to the reactions of the isotope in the Si detector. The centroid of the Gaussians was set to the value calculated from the range-energy table within a small margin. The final yield of an isotope with  $Z > 2$  was determined by correcting the yield evaluated from the moving source fit by the ratio between the two Gaussian yields and the linear background. Rather large systematic errors ( $\sim \pm 10\%$ ) are assigned for the multiplicity of IMFs before the background correction. These errors originate from the source fits which are evaluated from the different assumptions for the parameters, including individual sets for those isotopes with enough statistics. A total 13 data sets, in which the multiplicities of the isotopes with  $Z \leq 18$  are available, for different combinations of the projectile and target are used in this article.

### III. MODIFIED FISHER MODEL

To study the symmetry energy contribution to the fragment production, the MFM of Refs. [1,2] is used. In the MFM, the fragment yield of  $A$  nucleons with  $I = N - Z$ ,  $Y(A, I)$  is given by

$$Y(A, I) = CA^{-\tau} \exp\{[(W(A, I) + \mu_n N + \mu_p Z)/T] + N \ln(N/A) + Z \ln(Z/A)\}, \quad (1)$$

where  $C$  is a constant. The  $A^{-\tau}$  term originates from the entropy of the fragment, and the last two terms are from the entropy contributions for the mixing of two substances in the Fisher droplet model [22].  $\mu_n$  is the neutron chemical potential and  $\mu_p$  is the proton chemical potential, and  $W(A, I)$  is the free energy of the cluster at temperature  $T$ . As such, it includes both energy and entropy terms. In the model,

$W(A, I)$  is given by the following generalized Weizsäcker-Beth semiclassical mass formula [23,24] at a given temperature  $T$  and density  $\rho$ :

$$W(A, I) = -a_{\text{sym}}(\rho, T)I^2/A - a_c(\rho, T)Z(Z-1)/A^{1/3} + a_v(\rho, T)A - a_s(\rho, T)A^{2/3} - \delta(N, Z), \quad (2)$$

where the indexes  $v$ ,  $s$ ,  $c$ , and  $\text{sym}$  represent volume, surface, Coulomb, and symmetry energy, respectively. Following the semiempirical mass formulation, the pairing energy,  $\delta(N, Z)$ , is given by [25,26]

$$\delta(N, Z) = \begin{cases} a_p(\rho, T)/A^{1/2} & (\text{odd-odd}), \\ 0 & (\text{even-odd}), \\ -a_p(\rho, T)/A^{1/2} & (\text{even-even}). \end{cases} \quad (3)$$

We define the fragment yield ratio,  $R(I+2, I, A)$ , between isobars differing by 2 units in  $I$  as

$$\begin{aligned} R(I+2, I, A) &= Y(A, I+2)/Y(A, I) \\ &= \exp\{[W(I+2, A) - W(I, A) + (\mu_n - \mu_p)]/T \\ &\quad + S_{\text{mix}}(I+2, A) - S_{\text{mix}}(I, A)\}, \end{aligned} \quad (4)$$

where  $S_{\text{mix}}(I, A) = N \ln(N/A) + Z \ln(Z/A)$ . Hereafter, to simplify the description, the density and temperature dependence of the coefficients in Eq. (2) is omitted as  $a_i = a_i(\rho, T)$  ( $i = v, s, c, \text{sym}, p$ ). Inserting Eq. (2) into Eq. (4), one can get

$$\begin{aligned} R(I+2, I, A) &= \exp\{[\mu_n - \mu_p + 2a_c(Z-1)/A^{1/3} \\ &\quad - 4a_{\text{sym}}(I+1)/A - \delta(N+1, Z-1) \\ &\quad - \delta(N, Z)]/T + \Delta(I+2, I, A)\}, \end{aligned} \quad (5)$$

where  $\Delta(I+2, I, A) = S_{\text{mix}}(I+2, A) - S_{\text{mix}}(I, A)$ . One should note that  $\Delta(1, -1, A) = 0$  and for other  $I$  values  $\Delta(I+2, I, A) \leq 0.5$ , which is rather small comparing other parameters in Eq. (5).

Initially, we focus on the isobars with  $I = -1$  and 1. For these isobars the contributions from the symmetry term and the mixing entropy term in Eq. (5) drop out and, because these isobars are even-odd nuclei, the pairing term also drops out. Taking the logarithm of the resultant equation, one can get

$$\ln[R(1, -1, A)] = [(\mu_n - \mu_p) + 2a_c(Z-1)/A^{1/3}]/T. \quad (6)$$

For different reaction systems,  $N/Z$  and thus  $(\mu_n - \mu_p)/T$  can be different. To evaluate the system dependence of  $(\mu_n - \mu_p)/T$ , we determined the average value of  $\ln[R(1, -1, A)]$  over all available fragments for each system. In Fig. 2 these average values are plotted as a function of the entrance channel  $Z/A$  for the reaction systems studied. As seen in the figure, the average values show a linear dependence on the entrance channel  $Z/A$  of the system. Because the Coulomb energy in the right-hand side of Eq. (6) is that of the fragment itself and therefore expected to be very similar for the different reaction systems and the temperature  $T$  is also assumed to be similar because the same incident energy is used [27], we attribute the linear dependence seen in the figure to the difference of  $(\mu_n - \mu_p)/T$  in the different systems. Expressing  $(\mu_n - \mu_p)/T$  as

$$[(\mu_n - \mu_p)/T]_i = [(\mu_n - \mu_p)/T]_0 + \Delta\mu(Z/A)/T,$$

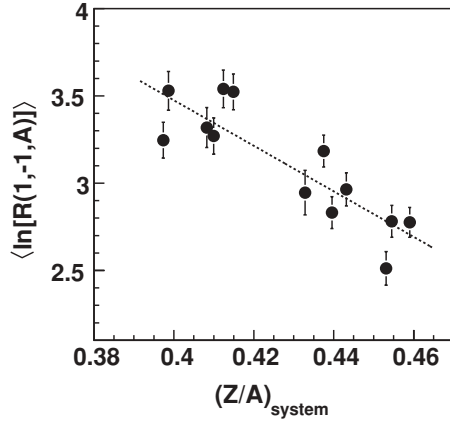


FIG. 2. Experimental average values of  $\ln[R(I+2, I, A)]$  for the case of  $I = -1$  are plotted as a function of  $Z/A$  of the reaction systems.  $Z/A = (Z_p + Z_t)/(A_p + A_t)$ , where  $p$  and  $t$  represent the projectile and the target, respectively. The dotted line is a linear fit.

and

$$\Delta\mu(Z/A)/T = c_1 \cdot (Z/A) + c_2,$$

here  $[(\mu_n - \mu_p)/T]_i$  denotes the value for a given reaction system  $i$ , and  $[(\mu_n - \mu_p)/T]_0$  is for the reference reaction system. A linear fit gives  $c_1 = -13.0$  and  $c_2 = 8.7$  for Fig. 2, in which the  $^{64}\text{Zn} + ^{112}\text{Sn}$  reaction is taken as the reference; that is, the extracted values in the figure have been adjusted to the reference reaction using  $\Delta\mu(Z/A)/T$ , in which  $\Delta\mu(Z/A)/T = 0$  for the  $^{64}\text{Zn} + ^{112}\text{Sn}$  reaction. In Fig. 3 the experimental values of  $\ln[R(1, -1, A)]$ , corrected by  $\Delta\mu(Z/A)/T$ , are plotted for all reactions as a function of  $A$ . Fitting these corrected average values using  $(\mu_n - \mu_p)/T$  and  $a_c/T$  as fitting parameters, Eq. (6) leads to  $(\mu_n - \mu_p)/T = 0.71$  and  $a_c/T = 0.35$ .

We next compare isobars with  $I = 1$  and 3, noting that these isobars are also even-odd nuclei for which the pairing term is 0.

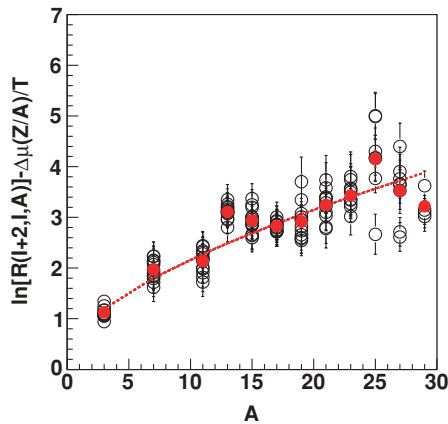


FIG. 3. (Color online) Experimental values of  $\ln[R(1, -1, A)]$  with the offset correction for different reactions is plotted as a function of  $A$  for  $I = -1$ . Open circles show results from the individual experiments and solid circles depict the average values for a given  $A$  over all reactions. The dotted line shows the result of fitting the average values with Eq. (6).

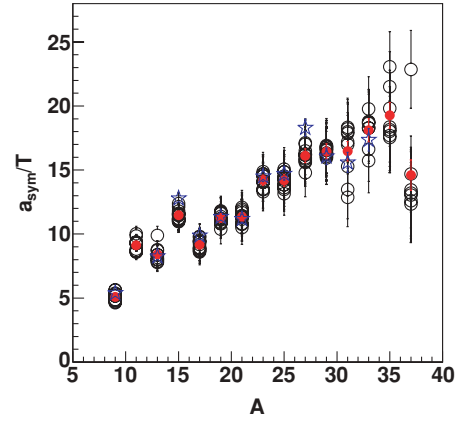


FIG. 4. (Color online) Experimental values of  $a_{\text{sym}}/T$  as a function of  $A$ . Open circles are obtained from Eq. (7) and solid circles are the average values for a given  $A$ . Stars are the average values obtained from Eq. (8).

For this combination, the symmetry energy coefficient term in Eq. (5) is given as a function of  $A$  by

$$a_{\text{sym}}/T = -A/8\{\ln[R(3, 1, A)] - [(\mu_n - \mu_p)/T + 2a_c(Z-1)/A^{1/3}]/T - \Delta\mu(Z/A)/T - \Delta(3, 1, A)\}. \quad (7)$$

In Fig. 4 values of  $a_{\text{sym}}/T$  calculated from Eq. (7) using the values  $(\mu_n - \mu_p)/T = 0.71$  and  $a_c/T = 0.35$  determined previously, are plotted as a function of  $A$ . All available values from the different reactions are plotted in the figure. The extracted values are very similar in magnitude and trend for the different reactions. In general, the values increase from 5 to  $\sim 16$  as  $A$  increases from 9 to 37 and may show a plateauing above that.

The symmetry term can also be extracted without evaluating the values of  $(\mu_n - \mu_p)/T$  and  $a_c/T$  explicitly. In Fig. 5, the experimental values of  $\ln[R(3, 1, A)]$  and  $\ln[R(1, -1, A)]$  from the  $^{64}\text{Zn} + ^{112}\text{Sn}$  reaction are plotted. The symmetry term,  $a_{\text{sym}}/T$ , for a given  $A$  can be extracted approximately

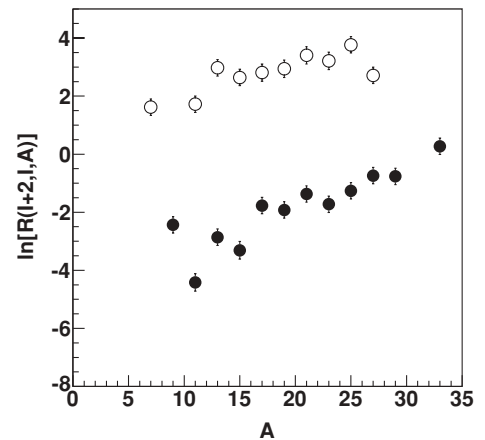


FIG. 5. Experimental values of  $\ln[R(I+2, I, A)]$  for  $I = -1$  (open circles) and  $I = 1$  (solid circles) for the  $^{64}\text{Zn} + ^{112}\text{Sn}$  reaction.

by the difference of these values as

$$a_{\text{sym}}/T \sim -A/8\{\ln[R(3, 1, A)] - \ln[R(1, -1, A)] - \Delta(3, 1, A)\}. \quad (8)$$

The approximation made in Eq. (8) is that the Coulomb term in  $\ln[R(3, 1, A)]$  is same as that in  $\ln[R(1, -1, A)]$ . In the actual calculation, the Coulomb term in  $\ln[R(3, 1, A)]$  for  $A = 13$ , for example, is calculated from the yield ratio of  $^{13}\text{B}/^{13}\text{C}$ , whereas that in  $\ln[R(1, -1, A)]$  is calculated from  $^{11}\text{B}/^{11}\text{C}$ , assuming that the ratio of the Coulomb energy for  $^{13}\text{B}/^{13}\text{C}$  is same as that of  $^{11}\text{B}/^{11}\text{C}$ . A similar approximation has been made for all extracted values. The resultant symmetry values are plotted in Fig. 4 using star symbols. The main difference between the values from Eq. (7) (circles) and those from Eq. (8) (stars) originates from the deviation of the data from the fitted line in Fig. 3.

The pairing terms in Eq. (5) can be determined using the extracted values for  $(\mu_n - \mu_p)/T$ ,  $a_c/T$ , and  $a_{\text{sym}}/T$  for the combination of isobars with  $I = 0$  and 2 and  $I = 2$  and 4. For  $I = 0$  and 2 isobars, the pairing term can be written as

$$a_p/T = (\text{sgn})\frac{1}{2}A^{1/2}\{\ln[R(2, 0, A)] - [(\mu_n - \mu_p) + 2a_c(Z-1)/A^{1/3} - 4a_{\text{sym}}/A]/T - \Delta(2, 0, A)\}, \quad (9)$$

and for  $I = 2$  and 4 it is given by

$$a_p/T = (\text{sgn})\frac{1}{2}A^{1/2}\{\ln[R(4, 2, A)] - [(\mu_n - \mu_p) + 2a_c(Z-1)/A^{1/3} - 12a_{\text{sym}}/A]/T - \Delta(4, 2, A)\}. \quad (10)$$

Here  $\text{sgn} = 1$  for  $(N, Z) = (\text{odd}, \text{odd})$  and  $-1$  for  $(\text{even}, \text{even})$  nucleus, in which  $A = N + Z$ .

The  $a_p/T$  values obtained from Eqs. (9) and (10), using the extracted values of  $(\mu_n - \mu_p)/T$ ,  $a_c/T$ , and  $a_{\text{sym}}/T$  given previously, are plotted in Fig. 6. In the top panel, for  $I = 0$  and 2 isobars, the pairing contribution is clearly observed for isobars with  $A < 30$ , though the even-odd oscillation pattern is slightly distorted. In the bottom panel, using Eq. (10) with  $I = 2$  and 4 isobars, the only clear pairing effect is observed for fragments only with  $A < 20$ .

The pairing term  $a_p/T$  can also be extracted from experimental yield ratios of isobars without the explicit evaluation of  $(\mu_n - \mu_p)/T$ ,  $a_c/T$ , and  $a_{\text{sym}}/T$ , similar to Eq. (8). Inserting Eqs. (6) and (8) into Eq. (9) with  $I = 0$  and 2 isobars, one can get

$$a_p/T \sim (\text{sgn})\frac{1}{2}A^{1/2}\{\ln[R(2, 0, A)] - \frac{1}{2}\{\ln[R(1, -1, A)] + \ln[R(3, 1, A)] - \Delta(3, 1, A)\} - \Delta(2, 0, A)\}. \quad (11)$$

From Eq. (10) with  $I = 2$  and 4 isobars,

$$a_p/T \sim (\text{sgn})\frac{1}{2}A^{1/2}\{\ln[R(4, 2, A)] + \frac{1}{2}\{\ln[R(1, -1, A)] - 3\ln[R(3, 1, A)] + 3\Delta(3, 1, A)\} - \Delta(4, 2, A)\}. \quad (12)$$

The resultant values are plotted in Fig. 6 using star symbols. These are the averaged values over all reactions. The results are consistent with those from Eqs. (9) and (10).

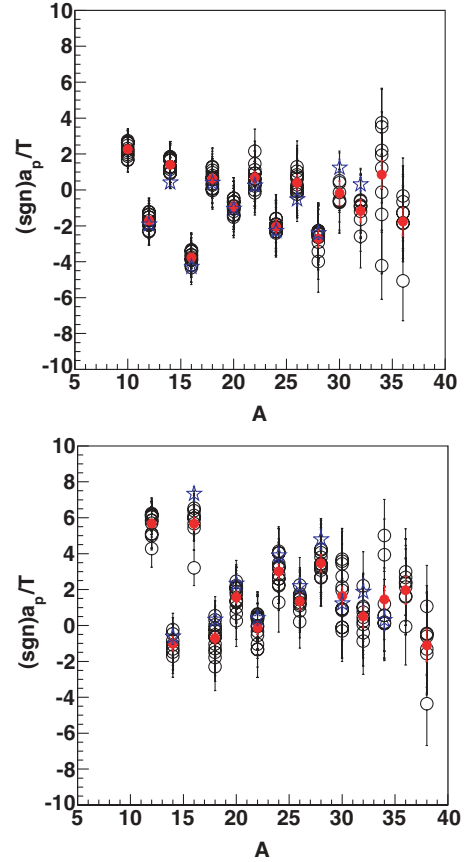


FIG. 6. (Color online) Extracted values of  $(\text{sgn})a_p/T$  are plotted as a function of  $A$ . Open circles are obtained in the top panel using Eq. (9) for individual reactions in the bottom panel using Eq. (10) for individual reactions. Solid circles are averaged values for a given  $A$  over all reactions. Stars are obtained from Eqs. (11) and (12).

#### IV. COMPARISONS WITH MODEL CALCULATIONS

In the multifragmentation regime of heavy-ion reactions, fragments may be formed in excited states [11,12]. Such fragments will deexcite by statistical decay processes. The experimentally detected fragments are normally in the ground state. To study the effect of the secondary decay process on the experimentally extracted symmetry energy coefficient, we have used an AMD code [9,16,17] to model the reaction dynamics and coupled it with the statistical decay code GEMINI [18] to model the secondary decay processes. The AMD code has been used to study the fragment production in Fermi-energy heavy-ion reactions and the global features of the experimental results have been well reproduced [28–33]. We believe that the dynamics can be crucial in accounting for fragment production in early stages of the reaction and the use of a dynamic model, such as AMD is essential.

Because the AMD calculation requires a lot of CPU time, only two of the experimental reaction systems have been studied in detail. The systems examined were  $^{64}\text{Zn} + ^{112}\text{Sn}$  and  $^{64}\text{Zn} + ^{124}\text{Sn}$ , both at 40 A MeV. All results shown in this article have been calculated using a newly installed computer cluster in the Cyclotron Institute [34]. The calculations have been performed, using the Gogny interaction with an

asymptotic stiff symmetry energy term [9], although very similar results are obtained for the standard Gogny interaction [35]. To obtain yields of the final products, the yields of primary fragments are first evaluated at a given time in the offline analysis. The fragments are formed using a coalescence radius,  $R_c$ , in phase space. Because the hot and dense composite system formed at an early stage of the reaction expands very quickly, the primary fragment distributions are rather sensitive to the choice of coalescence radius and the time of its application. When a smaller  $R_c$  is used, one can form fragments at an earlier stage. In previous calculations,  $R_c = 5$  and  $t = 300$  fm/c were used and the experimental results were well reproduced [29,31,32].  $R_c = 5$  corresponds to a radius of 5 fm in configuration space. To study the effect of the choice of these parameters, two different coalescence radii,  $R_c = 1.5$  and 5, are used here. In the case of  $R_c = 5$ , the fragment formation is evaluated at  $t = 300$  fm/c. For  $R_c = 1.5$ , the evaluation is at  $t = 150$  fm/c. The excitation energy of a fragment is calculated by subtracting the binding energy from the total energy. For each isotope the binding energy is calculated within the AMD code using a stochastic cooling method [36]. In the top panel of Fig. 7, the primary fragment distributions are shown as a function of the fragment  $Z$  for the two different cases. As one can see, for  $R_c = 1.5$ , the multiplicity of light IMFs with  $Z < 10$  is significantly enhanced, compared to that for  $R_c = 5.0$ , whereas the heavier fragment yields are suppressed as expected. The excitation of these primary fragments was followed using the GEMINI code [18]. The GEMINI code has been used extensively with

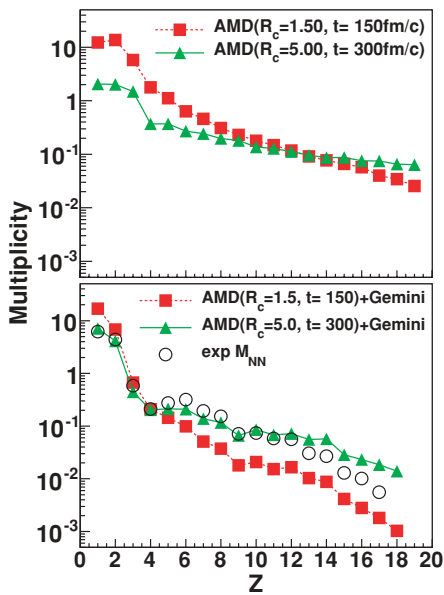


FIG. 7. (Color online) (Top) Calculated multiplicity distributions of the primary fragments evaluated using  $R_c = 1.5$  and 5. See details in the text. (Bottom) Multiplicity distributions of fragments for the experiments and the calculations. The experimental values are shown by open circles. The AMD + GEMINI calculated values filtered by the experimental acceptance are shown for  $R_c = 1.5$  (squares) and  $R_c = 5$  (triangles). All errors evaluated are smaller than the size of the symbols.

the AMD simulations in the past and good agreement with the experimental data has been seen [29,31,32]. To sample all possible decay channels of the excited fragments, one AMD event is used 100 times in GEMINI, with different random number seeds. In the bottom part of Fig. 7, the multiplicity distributions of the secondary fragments are compared with the experimental values. Because the experimental values are taken from the  $NN$ -source component of the energy spectra, the calculated energy spectra are subjected to the same filter. For simplicity, the calculated range of the impact parameter is set to  $0 < b < 8$  fm to suppress the contribution from the PLFs from the peripheral collisions. The impact parameter range was determined from the correlation between the collision centrality and impact parameter studied in Ref. [32]. The angle range, determined from the extracted moving source parameters, was set to  $5^\circ < \theta < 45^\circ$  to suppress the heavy projectilelike contribution and targetlike contributions. The experimentally observed multiplicity distribution for most particles, including  $Z = 1$  and 2, is well reproduced by the  $R_c = 5$  calculation. When  $R_c = 1.5$  is applied, the multiplicity is significantly overestimated for  $Z = 1$  and 2 and underestimated for  $Z > 4$ . In the case of  $R_c = 5$ , the calculated multiplicities start to deviate from those of the experiments at  $Z > 13$ , indicating that the projectilelike contribution becomes significant for these fragments.

Using the same prescription used for the experimental data,  $a_c/T$ ,  $a_{\text{sym}}/T$ , and  $a_p/T$  are evaluated from the filtered yields of isobars. In Fig. 8,  $\ln[R(I+2, I, A)]$  for the isobars with  $I = -1$  and 1 is plotted as a function of  $A$  for both primary and secondary fragments, together with the experimental results. No notable difference is observed between these. The calculated results are also well fitted by Eq. (6) and the values for  $(\mu_n - \mu_p)/T$  and  $a_c/T$  are extracted from the distributions of the primary and secondary isobars. The extracted values are  $(\mu_n - \mu_p)/T = 0.40$  and  $a_c/T = 0.18$  for the primary isobars

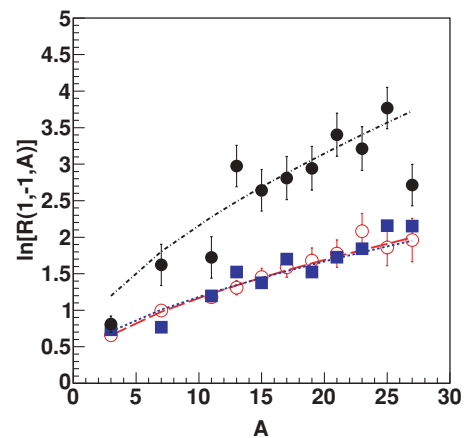


FIG. 8. (Color online)  $\ln[R(I+2, I, A)]$  for  $I = -1$  and 1 primary (open circles) and secondary (solid squares) fragments of AMD + GEMINI events for the  $^{64}\text{Zn} + ^{112}\text{Sn}$  reaction.  $\Delta\mu(Z/A)/T = 0$  for this reaction. Solid circles are the experimental values for this reaction. Dashed-dotted, dashed, and dotted lines show the fits for the experiments and the primary and the secondary fragments, using Eq. (6), respectively.

and  $(\mu_n - \mu_p)/T = 0.47$  and  $a_c/T = 0.17$  for those of the secondary (similar results are obtained from the unfiltered yields). The values following secondary decay should be compared to the experimental values of  $(\mu_n - \mu_p)/T = 0.71$  and  $a_c/T = 0.35$ . The calculated values of  $(\mu_n - \mu_p)/T$  both from the primary and secondary fragments are somewhat lower than that of the experiments.

AMD + GEMINI simulations reproduce only a half value of the experimental Coulomb term. The Coulomb term is not only related to the Coulomb coefficient, but also to the shape and density of the fragments at the time of their formation as well. In fact, the primary fragments produced by the AMD simulations have a shape far away from the spherical one. Because the fragments have odd shape, the density of the fragments is also difficult to be evaluated even from the simulations. However, the  $a_{\text{sym}}/T$  values extracted from Eq. (8), using two isobaric yield ratios from the simulations, are consistent with the values extracted from Eq. (7). In Eq. (8), both experimental ratios contain the same Coulomb term and they are canceled out. Therefore, the extracted  $a_{\text{sym}}/T$  values are independent of the Coulomb term and not affected by the discrepancy of the Coulomb terms shown in Fig. 8.

In Fig. 9,  $a_{\text{sym}}/T$  values evaluated using Eq. (7) with the values of  $(\mu_n - \mu_p)/T$  and  $a_c/T$  extracted from the model calculations are plotted as a function of  $A$ . The average values of the experimental results from Fig. 4 (solid circles) should be compared with those extracted following the deexcitation step in the GEMINI code (open circles). Although the experimental values show larger fluctuations, the calculated values and the data are in good agreement in magnitude and trend. In the figure the values extracted from the primary fragment yields are also plotted for both  $R_c = 1.5$  (squares) and 5 (triangles). The values for  $R_c = 5$  show a slowly increasing distribution as a function of  $A$  with  $a_{\text{sym}}/T \sim 4$  to 5 up to  $A \sim 30$ . Those for  $R_c = 1.5$  show a similar trend, but the values are

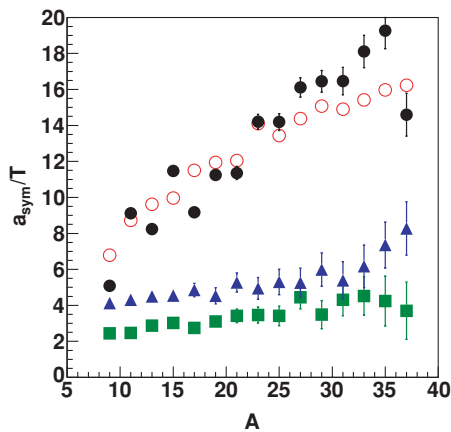


FIG. 9. (Color online) Extracted values of symmetry energy coefficient from the experiments (solid circles) and calculations from the secondary fragments for  $R_c = 5$  (circles). Squares and triangles show those obtained for primary fragments for  $R_c = 1.5$  and  $R_c = 5$ , respectively. All errors evaluated are smaller than the size of the symbols.

smaller. The rather flat distribution of  $a_{\text{sym}}/T$  values of the primary fragments for  $A < 30$  is consistent with a scenario of fragment emission from a common source with a given density and temperature. The heavier fragments with  $A > 30$  may result from different mechanisms, for example, projectile fragmentation in the more peripheral collisions.

The pairing effect is experimentally observed in Fig. 6, especially from the ratios of  $I = 0$  and 2 isobars in the upper panel. In the study of the complex fragments production in the  $^{238}\text{U} + \text{Ti}$  reaction at 1 A GeV, Ricciardi *et al.* suggested that the observed even-odd oscillation in the fragment yields originates from the last chance particle decay of the excited fragments during their cooling-down evaporation process [37,38]. To verify this hypothesis in our experiment, we also did a similar study, using AMD + GEMINI calculations. Three sets of simulated events were prepared. In the first set, all fragments were in the final ground state. In the second set, the last chance particle decay was blocked and all fragments were in an excited state just before the last chance particle decay. In the third set, the last two particles decays are blocked. In the actual calculations, the second set was generated from the first set by adding the charge and mass of the last chance emitted particle to that of the partner IMF. Similarly, the third set was generated by adding the charge and mass of the last two emitted particles to that of the partner IMF. In Fig. 10, the results from Eq. (9) are shown in the top panel and those from Eq. (10) for the different fragment sets are shown in the bottom panel. As one can see in the top panel, the values calculated from the ratios of  $I = 0$  and 2 isobars in the ground state (triangles) show clearly the same even-odd oscillation pattern as those in the top panel of Fig. 6 and the pattern is significantly reduced for the fragments just before the last particle decay (circles). The oscillation is totally washed out for those from the third set of fragments (squares), indicating that the even-odd pattern is generated at the end of the deexcitation of the excited fragments. The size of the oscillation for the final products are comparable to those observed in the top panel of Fig. 6. Even the disappearance of oscillations above  $A = 30$  is well reproduced. However, in the results from Eq. (10) for isobars of  $I = 2$  and 4 in the ground states (triangles) the oscillation pattern is observed at  $20 \geq A \geq 30$ , whereas for the experimental results, as seen in the bottom panel of Fig. 6, the pattern is observed for  $A \leq 20$ , though the oscillation pattern is the same. Furthermore, the pattern is sustained for those from the last chance particle decay with opposite even-odd pattern (circles). This oscillation pattern is significantly reduced for those before the last two particle decays (squares). The average offset of the  $a_p/T$  values are also 3–4 units above zero in the calculation and 2–3 units above in the experimental results in the bottom panel of Fig. 6. Ricciardi *et al.* reported that the even-odd effect appears strongest for  $I = 0$  fragments for even-mass nuclei and it becomes strongest for  $I = 5$  for odd mass nuclei. These facts may complicate the even-odd effect for isobars of  $I = 2$  and 4 during the cascade. However, all the oscillation patterns observed in our simulations, either from isobars of  $I = 0$  and 2 or from those of  $I = 2$  and 4, are generated at the end of the deexcitation process of the excited fragments and they are reduced significantly for the second or third sets of the

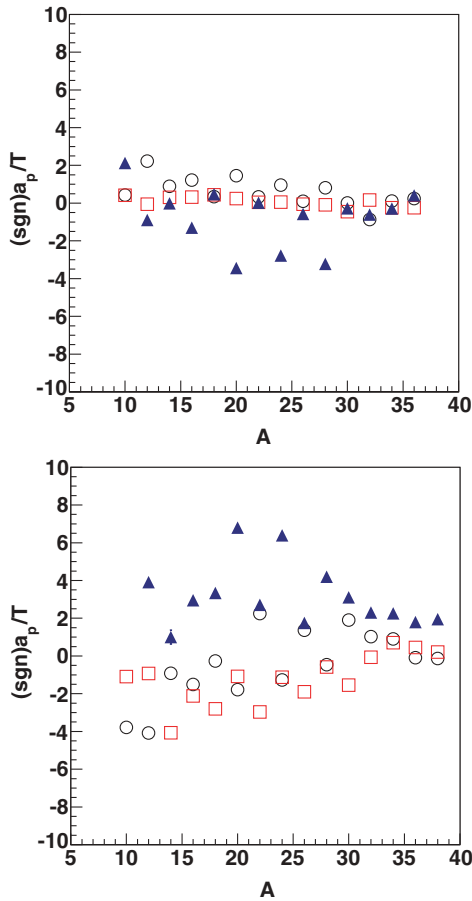


FIG. 10. (Color online) Calculated  $a_p/T$  values from different sets of fragments for  $I = 0, 2$  (top) and  $I = 2, 4$  (bottom). Triangles show results for fragments in the ground states; circles are for those in excited states just before the last particle decay. Squares are for those in excited states before the last two particle decays.

fragments, which is consistent to the hypothesis proposed by Ricciardi *et al.* [37,38].

## V. SUMMARY

For a large series of heavy-ion reactions, coefficients of Coulomb energy, symmetry energy and pairing energy in the form of  $a_i/T$  as a function of  $A$  have been studied from analyses of the yield ratios of isobars obtained in experiments and from model calculations. The AMD and GEMINI codes were used for the calculations. For the symmetry energy term, the extracted values from the experiments are in good agreement with those calculated for the final fragments in the ground state. They increase from 5 to  $\sim 16$  as the masses of the fragments increase from 9 to 37. These values are generally much larger than those extracted from the primary fragments observed in the AMD calculations. Over the same mass interval the primary fragment values range from 4 to 5. This is consistent with a picture in which the primary fragments originate from a common emitting source. A smaller coalescence radius and earlier sampling time for the fragment

formation in the AMD calculation results in slightly smaller values of 2 to 3 for the primary fragments, but does not have a strong effect on the extracted values for the final fragments, though the fragment yield distribution is not well reproduced compared to the case of  $R_c = 5$ . Although the technique employed is quite different, our model results are quite similar to those observed by Ono where the ratio  $\zeta(Z) = C_{\text{sym}}/T$  was extracted from the variance of the calculated isotope distributions for the reactions  $^{40}\text{Ca} + ^{40}\text{Ca}$ ,  $^{48}\text{Ca} + ^{48}\text{Ca}$ , and  $^{60}\text{Ca} + ^{60}\text{Ca}$  at 35 A MeV [35]. In that article the ratios are evaluated from the quadratic shapes of the isotope distributions for a given  $Z$  after proper normalization of the isotopic yields from the three different reactions. The comparisons between the experimentally extracted results and those of the calculations indicate that the experimental determination of symmetry energy coefficients,  $a_{\text{sym}}/T$ , are significantly affected by the secondary decay processes of the primary fragments. This modification is a common feature of dynamic transport model approaches [35,39]. In the aforementioned study of Ono, the effect of the different effective interactions for the symmetry energy has also been studied, using the standard Gogny ( $g0$ ) and that with asymptotic stiff symmetry energy ( $g0AS$ ), and it was found that the difference in the symmetry term between the two different interactions is rather small for both the primary and the secondary fragments, compared to the significant change of the  $Z$  dependence between the primary and the secondary fragments as observed in Fig. 9. Thus extraction of the density dependence of the symmetry energy from fragment observables must be done with caution and with appropriate attention to the role of the secondary decay. The importance of these effects will vary according to the observables employed for extraction of the desired information.

The pairing effect is clearly observed in the experiments. Comparisons to the calculations strongly support the hypothesis, which is proposed by Ricciardi *et al.* [37,38], that the observed effect originates at the end of the statistical cooling-down process of the excited fragments.

The Coulomb coefficient in the form of  $a_c/T$  is also evaluated in both the experiment and the calculations. The experimentally extracted value is  $a_c/T = 0.35$ , whereas the calculated values are  $a_c/T = 0.17$  for the final fragments and  $a_c/T = 0.18$  for the primary fragments. These differences suggest that the calculated fragments are more deformed and/or expanded than those observed in the experiments.

## ACKNOWLEDGMENTS

We thank the staff of the Texas A&M Cyclotron facility for their support during the experiment. We also thank L. Sobotka for letting us to use his spherical scattering chamber. We further thank A. Ono and R. J. Charity for providing us their simulation codes. This work was supported by the US Department of Energy under Grant No. DE-FG03-93ER40773 and the Robert Welch Foundation under Grant A0330. Z. Chen also thanks the ‘‘100 Persons Project’’ of the Chinese Academy of Sciences for the support.

- [1] R. W. Minich, S. Agarwal, A. Bujak, J. Chuang, J. E. Finn, L. J. Gutay, A. S. Hirsch, N. T. Porile, R. P. Scharenberg, B. C. Stringfellow, and F. Turkot, *Phys. Lett. B* **118**, 458 (1982).
- [2] A. S. Hirsch, A. Bujak, J. E. Finn, L. J. Gutay, R. W. Minich, N. T. Porile, R. P. Scharenberg, B. C. Stringfellow, and F. Turkot, *Nucl. Phys. A* **418**, 267c (1984).
- [3] S. Kowalski *et al.*, *Phys. Rev. C* **75**, 014601 (2007).
- [4] B. A. Li, *Phys. Rev. C* **67**, 017601 (2003).
- [5] A. Bonasera *et al.*, *Phys. Rev. Lett.* **101**, 122702 (2008).
- [6] H. S. Xu *et al.*, *Phys. Rev. Lett.* **85**, 716 (2000).
- [7] M. B. Tsang *et al.*, *Phys. Rev. C* **64**, 054615 (2001).
- [8] A. S. Botvina, O. V. Lozhkin, and W. Trautmann, *Phys. Rev. C* **65**, 044610 (2002).
- [9] A. Ono, P. Danielewicz, W. A. Friedman, W. G. Lynch, and M. B. Tsang, *Phys. Rev. C* **68**, 051601(R) (2003).
- [10] A. Kelić, J. B. Natowitz, and K. H. Schmidt, *Eur. Phys. J. A* **30**, 203 (2006).
- [11] N. Marie *et al.*, *Phys. Rev. C* **58**, 256 (1998).
- [12] S. Hudan *et al.*, *Phys. Rev. C* **67**, 064613 (2003).
- [13] R. Wada *et al.*, Annual Report of the Cyclotron Institute, Texas A&M University, 2005, II-3 (unpublished), available at <http://cyclotron.tamu.edu/publications.html>.
- [14] L. G. Moretto, C. O. Dorso, J. B. Elliott, and L. Phair, *Phys. Rev. C* **77**, 037603 (2008).
- [15] S. Albergo, S. Costa, E. Costanzo, and A. Rubbino, *Nuovo Cimento A* **89**, 1 (1985).
- [16] A. Ono and H. Horiuchi, *Phys. Rev. C* **53**, 2958 (1996).
- [17] A. Ono, *Phys. Rev. C* **59**, 853 (1999).
- [18] R. J. Charity *et al.*, *Nucl. Phys. A* **483**, 371 (1988).
- [19] Ad. R. Raduta and F. Gulminelli, *Phys. Rev. C* **75**, 044605 (2007).
- [20] Z. Chen *et al.*, [arXiv:1002.0319](https://arxiv.org/abs/1002.0319).
- [21] F. Hubert, R. Bimbot, and H. Gauvin, *At. Data Nucl. Data Tables* **46**, 1 (1990).
- [22] M. E. Fisher, *Rep. Prog. Phys.* **30**, 615 (1967).
- [23] C. F. von Weizsäcker, *Z. Phys.* **96**, 431 (1935).
- [24] H. A. Bethe, *Rev. Mod. Phys.* **8**, 82 (1936).
- [25] A. E. S. Green and D. F. Edwards, *Phys. Rev.* **91**, 46 (1953).
- [26] M. A. Preston, *Physics of the Nucleus* (Addison-Wesley, Reading, MA, 1962).
- [27] J. Wang *et al.*, *Phys. Rev. C* **72**, 024603 (2005).
- [28] A. Ono, S. Hudan, A. Chbihi, and J. D. Frankland, *Phys. Rev. C* **66**, 014603 (2002).
- [29] R. Wada *et al.*, *Phys. Lett. B* **422**, 6 (1998).
- [30] A. Ono and H. Horiuchi, *Prog. Part. Nucl. Phys.* **53**, 501 (2004).
- [31] R. Wada *et al.*, *Phys. Rev. C* **62**, 034601 (2000).
- [32] R. Wada *et al.*, *Phys. Rev. C* **69**, 044610 (2004).
- [33] S. Hudan, R. T. de Souza, and A. Ono, *Phys. Rev. C* **73**, 054602 (2006).
- [34] R. Wada, M. Huang, R. Burch, and K. Hagel, Annual Report of the Cyclotron Institute, Texas A&M University, 2009, V-45 (unpublished), available at <http://cyclotron.tamu.edu/publications.html>.
- [35] A. Ono, [arXiv:nucl-th/0605003v1](https://arxiv.org/abs/nucl-th/0605003v1).
- [36] A. Ono, H. Horiuchi, T. Maruyama, and A. Ohnishi, *Prog. Theor. Phys.* **87**, 1185 (1992).
- [37] M. V. Ricciardi *et al.*, *Nucl. Phys. A* **733**, 299 (2004).
- [38] M. V. Ricciardi *et al.*, *Nucl. Phys. A* **749**, 122c (2005).
- [39] T. X. Liu *et al.*, *Phys. Rev. C* **69**, 014603 (2004).